ACADEMIA ROMÂNĂ
Revue Roumaine de Chimie
https://www.icf.ro/rrch/

Rev. Roum. Chim.,
2024, *69*(5–6), 291–300
DOI: 10.33224/rrch.2024.69.5-6.07

*Dedicated to Professor Vasile P**â**rvulescu*
on the occasion of his 70th anniversary

THE INFLUENCE OF THE PRECURSOR TYPE IN THE SYNTHESIS OF Mg/Al-HYDROTALCITE THROUGH A NON-TRADITIONAL METHOD USED FOR CLAISEN–SCHMIDT CONDENSATION

Rodica ZĂVOIANU,[a,b,*] Bogdan E. COJOCARU,[a,b] Sabina G. ION,[a,b] Ana Paula SOARES DIAS,[c] Anca CRUCEANU[a,b] and Octavian D. PAVEL[a,b,*]

[a]University of Bucharest, Faculty of Chemistry, Department of Inorganic & Organic Chemistry, Biochemistry and Catalysis, 4–12 Regina Elisabeta Blv., 030018, Bucharest, Roumania
[b]Research Center for Catalysts & Catalytic Processes, Faculty of Chemistry, University of Bucharest, Roumania
[c]Univ Lisbon, CERENA, Inst Super Tecn, Ave Rovisco Pais 1, P-1049001 Lisbon, Portugal

Received March 5, 2024

Traditionally, the synthesis of MgAl-hydrotalcite is performed in the presence of inorganic alkalis-type precipitating agents using the co-precipitation method. As an viable alternative, the use of organic alkalis and the mechanochemical method can remove some of the issues that the traditional route generates, *i.e.* the possibility of final solid contamination with alkaline cations; a high energy consumption, relative to the amount of water used but also of electric current; the involvement of a large number of utensils necessary for the synthesis; time allocated to the solid preparation; etc. Changing the regular precursor type (*i.e.* nitrate) of the target cation with chloride or sulfate leads to obtaining hydrotalcites which have different basicities. The chlorides precursors lead to the synthesis of materials that show a better ability for the reconstruction of the layered structure. Moreover, TMAH acts both as a synthesis agent and as a templating agent. The tight pore distribution is characteristic of all materials obtained from chloride precursors, where the co-precipitation method generates pores of 97Å, while the mechanochemical method generates pores of 140Å. The material with the highest catalytic activity for Claisen-Schmidt condensation, conversion of 92%, is the one obtained by calcination of the hydrotalcite prepared from chloride precursors by the mechanochemical method, while the co-precipitation method leads to conversions of 90%. The novelty of this work is that these type of catalysts obtained from chlorides or sulfate precursors in presence of TMAH have not been used in Claisen-Schmidt condensation until now.

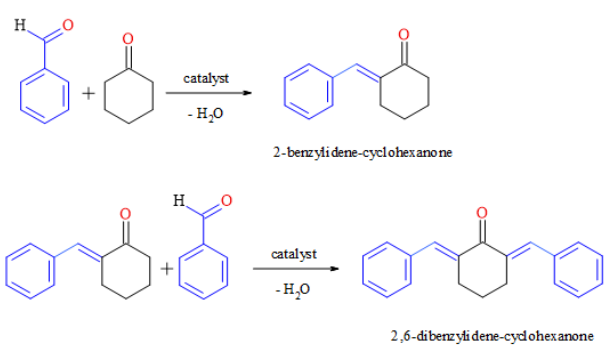

INTRODUCTION

Recently, layered double hydroxides (LDH) have found utility in different important areas, *i.e.* catalysts for the synthesis of fine chemicals,[1] in environmental protection as adsorbents,[2] as corrosion inhibitors,[3] as polymer additives,[4] etc. Their general formula $[M^{2+}_{1-x}M^{3+}_{x}(OH)_2]^{x+}[A^{n-}_{x/n}]\cdot mH_2O$[5] (where M^{2+}, M^{3+}

* Corresponding author: rodica.zavoianu@chimie.unibuc.ro; octavian.pavel@chimie.unibuc.ro

are *bi* - and *tri*-valent cations adopting an octahedral geometry, *A* is an anion with charge *n*, *x* is equal to the ratio $M^{3+}/(M^{2+} + M^{3+})$, *m* is the water molecules number), allows incorporation of multiple / different types of *bi*- and *tri*-valent cations, thus generating ternary or quaternary compounds. A peculiar property of LDH is the memory effect which allows the reconstruction of the layered structure by hydrating the mixed oxides obtained by calcination of the parent LDH up to 500–600 °C with water / an aqueous solution containing a target compensation anion. A higher calcination temperature favors the migration of cations from octahedral positions to tetrahedral ones, leading to the loss of memory effect. The reconstruction of parent structure was explained by two mechanisms: (i) a dissolution–recrystallization process suggested by Ulibarri and Takehira[6,7] and (ii) retro–topotactic transformation, proposed by Marchi and Apesteguía.[8] Based on the memory effect, it is also possible to insert different anions that present large dimensions,[9] but also the change in the carbonate / hydroxyl ratio.[10] Usually, the hydrotalcite materials can be synthesized by several methods, *i.e.* co-precipitation (at low / high supersaturation or urea hydrolysis),[11,12] ion-exchange,[13] rehydration using structural memory effect,[14] hydrothermal method,[15] secondary intercalation,[16] etc. Newer trends include: mechanochemical synthesis,[17] exfoliation in aqueous solution,[18] electrochemical synthesis,[19] etc. The inorganic alkalis (*i.e.* K_2CO_3, KOH, NaOH, Na_2CO_3, NH_4OH, etc.) are usually involved as precipitating agent. However, their presence often contaminates the final material with alkaline cations. In order to eliminate this drawback, a new approach considers the utilization of organic alkalis as precipitation agent[17,20–22] which, in addition to the absence of the alkaline cation, also leads to a decrease in the amount of water used in washing step of the synthesis. The organic alkalis also present some disadvantages, considering their cost compared to inorganic alkalis, an inadequate solubility in water which is accentuated with the growth of the hydrocarbon chain or the tendency to be decomposed during the LDH synthesis.

The Claisen-Schmidt condensation reaction is one of the most important reactions for the synthesis of a very wide spectrum of key compounds as well as their derivatives, which have found their use as antioxidants, dyes, medicinal compounds, pigments, food additives, pesticides, etc.[23] Thus, the condensation of cyclohexanone and benzaldehyde generates two types of compounds: *i.e. mono*-condensed (2-benzylidene-cyclohexanone) and *di*-condensed (2,6-dibenzylidene-cyclohexanone),[24] which are important for *anti*-cancer drugs or as precursors for *anti*-inflammatory drugs. The ratio between both compounds has been tried to be explained over time, but opinions are still divided.[25,26]

The aim of this article is: (i) to determine the influence of the nature of the precursors (sulfate / chloride) on the physico-chemical properties of Mg/Al hydrotalcite; (ii) the assessment of the effect produced by using organic alkalis as precipitation agent (TMAH – Tetra Methyl Ammonium Hydroxide) and the mechanochemical synthesis method; (iii) bringing new arguments regarding the *mono*-/*di*- condensed products ratio.

EXPERIMENTAL

1. Preparation of the catalysts

1.1. Mg/Al-hydrotalcite synthesis using chloride as precursors.

The synthesis of solids was carried out at a pH of 10 under low super-saturation conditions using a solution containing 1.5 M of Mg^{2+} and Al^{3+} chloride (0.2 mol Mg^{2+} / 0.0666 mol Al^{3+}) in *bi*-distilled water, and a volume of TMAH solution to reach the desired pH value. Both solutions were simultaneously added with TIM854, NB pH/EP/Stat pH-STAT Titrator in a batch reactor at a feed flow of 60 $mL \cdot h^{-1}$, under room temperature (RT) and vigorous stirring of 600 $rot \cdot min^{-1}$. The obtained gel was aged 18 h at 75 °C, cooled to RT, filtered and washed with *bi*-distilled water until pH of 7. The drying of the hydrotalcite gel was performed at 120 °C for 24 h in air atmosphere, the sample being named HT-TMAH-Cl^--CP. The corresponding mixed oxide was obtained via the calcination of hydrotalcite at 460 °C for 18 h in an air atmosphere (cHT-TMAH-Cl^--CP). The reconstruction of the layered structure by memory effect was performed by impregnation of the mixed oxides with *bi*-distilled water for 24 h. The reconstructed solids were then separated by filtration and dried at 90 °C for 24 h in the air atmosphere (hyHT-TMAH-Cl^--CP). For the mechanochemical method, the required amounts of Mg and Al chlorides as well as TMAH were mixed directly in a Mortar Grinder RM 200 for 1h in the absence of water addition. The obtained white paste was then washed (with no aging step presence) with *bi*-distillated water until the neutral pH value. The drying was performed at 120 °C for 24 h in air atmosphere with obtaining of HT-TMAH-Cl^--MC sample. The calcination and reconstruction were carried out following the same procedure as for co-precipitated samples, yielding the samples: cHT-TMAH-Cl^--MC; hyHT-TMAH-Cl^--MC.

1.2. Mg/Al-hydrotalcite synthesis using sulfate as precursors

The synthesis was carried out following a similar path to the one employed with chloride precursors but this time the precursors were Mg and Al sulfates. The samples were annotated as follows: HT-TMAH-SO_4^{2-}-CP; cHT-TMAH-SO_4^{2-}-CP; hyHT-TMAH-SO_4^{2-}-CP; HT-TMAH-SO_4^{2-}-MC; cHT-TMAH-SO_4^{2-}-MC; hyHT-TMAH-SO_4^{2-}-MC.

2. Characterization of the catalysts

Powder X-ray diffraction (XRD) patterns were recorded with a Shimadzu XRD 7000 diffractometer equipped with a source of CuK$_\alpha$ radiation (λ = 1.5418 Å, 40 kV, 40 mA) with a scanning speed conditions of 0.10°·min^{-1} in the 2θ range of 5–80°. The Diffuse Reflectance Infrared Fourier Transform Spectroscopy (DRIFT) spectra were recorded by JASCO FT/IR-4700 LE spectrometer, using an accumulation of 400 scans in the 400–4000 cm^{-1} range. Diffuse reflectance UV-Vis spectra (DR-UV-Vis) were recorded with a Jasco V–650 UV-Vis spectrophotometer equipped with an integration sphere in the range 900–200 nm, using Spectralon as a white reference. The textural properties were obtained by N_2 adsorption-desorption isotherms using a Micromeritics ASAP 2010 apparatus. The basicity of samples were determined by the irreversible titration using organic molecules with different pK_a values, *i.e.* phenol pK_a = 9.9 and acrylic acid, pK_a = 4.2.[27]

3. Catalytic tests

Claisen-Schmidt condensation (Scheme 1) was performed under batch conditions. 0.002 moles of benzaldehyde was mixed with 0.001 moles of cyclohexanone (both from Sigma-Aldrich, > 99%) under solvent-free conditions. When the temperature was stabilized at 120 °C, 20 mg of catalysts were added, and the reaction was carried out 2 h.[27] After completing, 1 mL of toluene was inserted for products solubilization, followed by filtration of catalyst and analysis of liquid mixture by Thermo-Quest Gas Chromatograph with a FID detector and a capillary column of 30 m length having the DB5 as stationary phase. GC/MS/MS Varian Saturn 2100 T was also used for identification of the products.

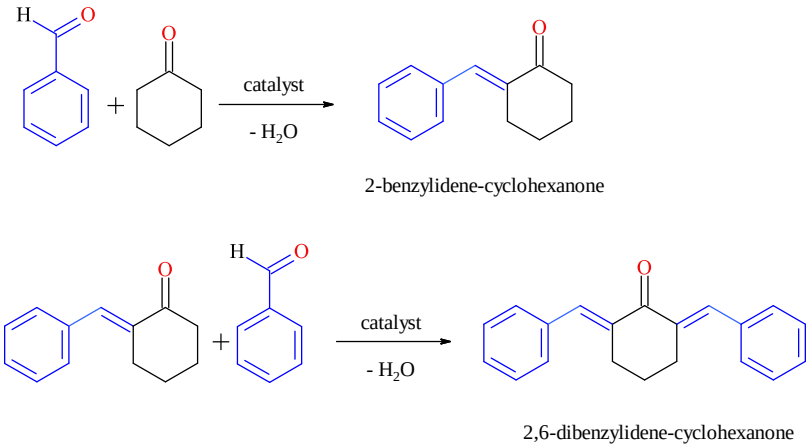

Scheme 1 – Claisen-Schmidt condensation of benzaldehyde and cyclohexanone to mono-condensed product (2-benzylidene-cyclohexanone) and di-condensed product (2,6-dibenzylidene-cyclohexanone).

RESULTS AND DISCUSSION

1. Catalysts characterization

1.1. XRD characterization. Figure 1A-D (black lines) shows the typical patterns of hydrotalcite structure where the *003*, *006*, *110* and *113* planes showed sharp and symmetric reflexions, while *012*, *015* and *018* planes were broad and asymmetric.

The positive effect of the mechanochemical method is highlighted for the sample obtained from sulfate-type precursors because there are no lines corresponding to other impurity phases present in the X-ray diffractogram (Fig. 1D). Meanwhile, for the sample prepared by co-precipitation method, the lines corresponding to $Mg(OH)_2$ were noticed (Fig. 1C). The use of chloride precursors leads to the presence of Mg and Al hydroxides impurity phases, regardless of the method type used (Fig. 1A, B). The mixed oxides obtained by calcination of the parent hydrotalcites do not show the MgO impurity for the samples prepared from sulfates (Fig. 1C, D red lines), while the calcined samples obtained from chloride precursors show diffraction lines corresponding to MgO (Fig. 1A, B red lines). Their presence is explained by the fact that $Mg(OH)_2$ present as impurity phase in the hydrotalcite samples transforms into oxide phase. Moreover, MgO also remains as stable phase during reconstruction, fact highlighted by presence of the corresponding line in the XRD patterns of reconstructed sample (blue lines). The layered structure was not fully reconstructed because the diffraction lines are of a lower intensity compared to those of the parent hydrotalcite. However, the chlorides precursors generated materials that presented a better ability of reconstruction by memory effect than that of the materials obtained from sulfates as precursors. Since there are only two types of cations, *i.e.* Mg and Al involved, the network parameter ***a*** (corresponding to cation – cation distance) don't present an important variation, *e.g.* between 3.0348 and 3.0792. Instead, the IFS network parameter (corresponding to interlayer space) shows a significant variation, showing a decrease from hydrotalcite to

reconstructed samples. Such a behavior is explained by the insertion of a larger amount of hydroxyl groups in the interplanar space than CO_3^{2-}, a fact also certified by literature.[10]

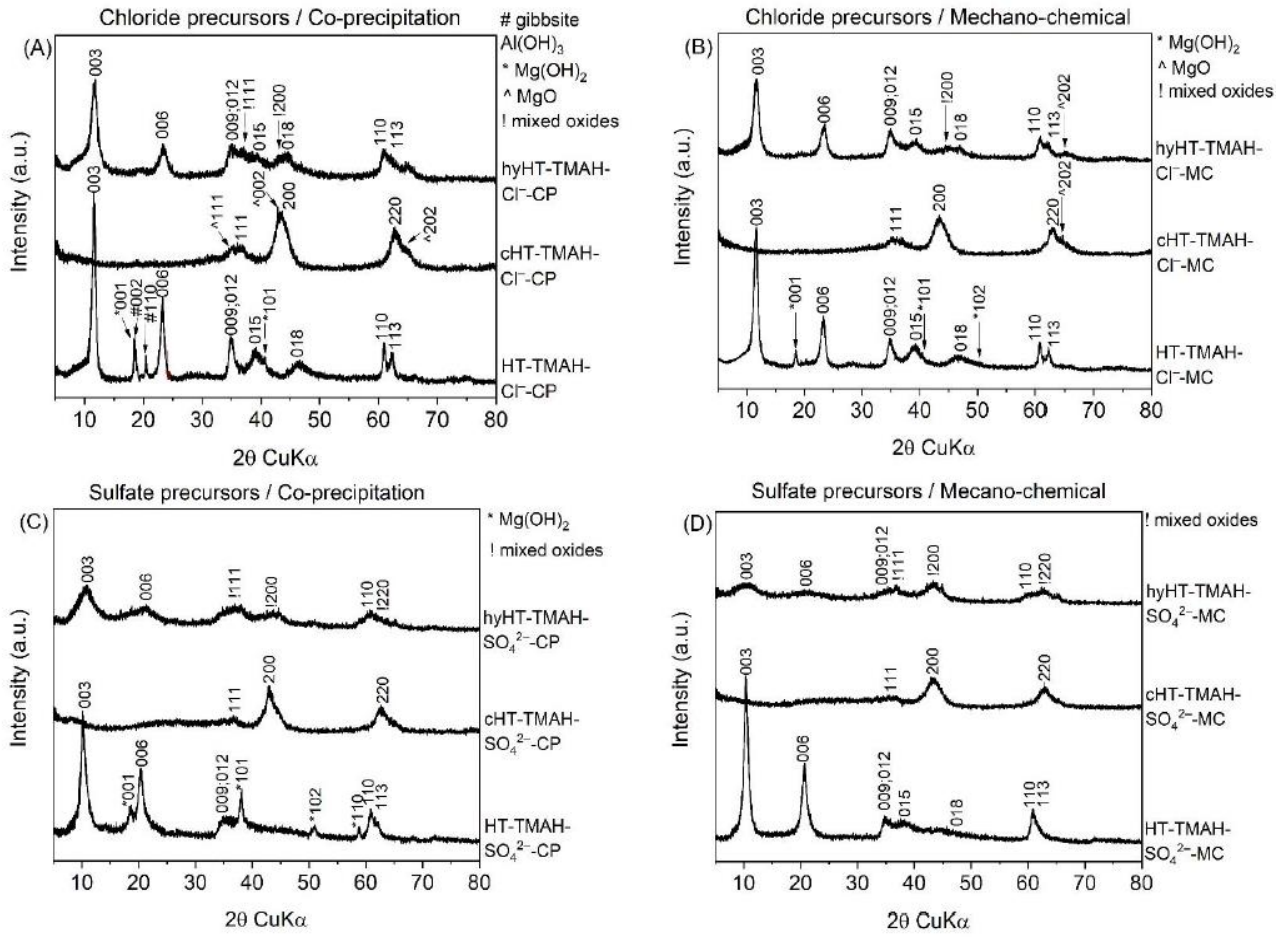

Fig. 1 – The XRD patterns of samples prepared by: co-precipitation from chlorides as precursors (A); mechanochemical from chlorides as precursors (B); co-precipitation from sulfates as precursors (C); and mechanochemical from sulfates as precursors (D).

Table 1

The network parameter of samples prepared with TMAH by co-precipitation / mechanochemical methods

Hydrotalcite samples	**Lattice parameters**		**IFS***	**2 θ$_{003}$ (°)**	**FWHM$_{003}$**	**FWHM$_{110}$**	**D**	**(Å)**
	***a* (Å)**	***c* (Å)**	**(Å)**					
HT-TMAH-Cl⁻-CP	3.0386	22.9489	2.85	11.5729	0.7593	0.8033	105.24	
hyHT-TMAH-Cl⁻-CP	3.0454	22.7951	2.80	11.6350	1.3100	1.0400	61.00	
HT-TMAH-SO_4^{2-}-CP	3.0427	24.5324	3.38	11.5327	1.4820	0.9400	98.76	
hyHT-TMAH-SO_4^{2-}-CP	3.0454	24.4194	3.34	11.5893	1.2200	1.6100	69.77	
HT-TMAH-Cl⁻-MC	3.0454	23.3899	2.99	10.2528	0.8091	0.6360	75.14	
hyHT-TMAH-Cl⁻-MC	3.0445	22.8882	2.83	10.5800	1.1453	0.8934	27.34	
HT-TMAH-SO_4^{2-}-MC	3.0348	24.7041	3.43	10.4044	1.2350	1.0300	85.20	
hyHT-TMAH-SO_4^{2-}-MC	3.0792	23.6088	3.07	10.6650	0.8666	1.6266	194.75	
Mixed oxides samples	***a* (Å)**			**2 θ$_{200}$ (°)**	**FWHM$_{200}$**		**D***	**(Å)**
cHT-TMAH-Cl⁻-CP	4.1831			43.2200	1.7734		48.22	
cHT-TMAH-SO_4^{2-}-CP	4.1561			43.5150	1.8600		34.37	
cHT-TMAH-Cl⁻-MC	4.1841			43.2100	2.4900		45.97	
cHT-TMAH-SO_4^{2-}-MC	4.1611			43.4600	2.5734		33.25	

*IFS represents the interlayer free distance

**D represents the mean crystallite size (derived from the Debye-Scherrer equation) determined from the FWHM of the (003) reflection for LDH samples

***D represents the mean crystallite size (derived from the Debye-Scherrer equation) determined from the FWHM of the (200) reflection for mixed oxides

1.2. DRIFT characterization

The DRIFTS spectra (Fig. 2A–D), present the band at 3700 cm^{-1} corresponding to OH group vibration in Mg-OH type phase, highlighted in XRD. Also, a wide band at 3700–3400 cm^{-1} corresponds to the OH group vibration, ν(O–H), while that at 3000 cm^{-1} relates to the hydrogen bonds between water and carbonate in the interlayer space. The band at 1664–1628 cm^{-1} is due to the H_2O bending vibration of interlayer water in the layered structure, that between 1100 cm^{-1} and 650 cm^{-1} were assigned to the CO_3^{2-} group vibration, while those below of 600 cm^{-1} correspond to Mg–O and Al–O bonds. The band at 2040–2095 cm^{-1} is attributed to *tri*-methylamine (an impurity from TMAH) and linearly adsorbed CO. By calcination at 460 °C *tri*-methylamine undergoes a decomposition process while linearly adsorbed CO is still present.

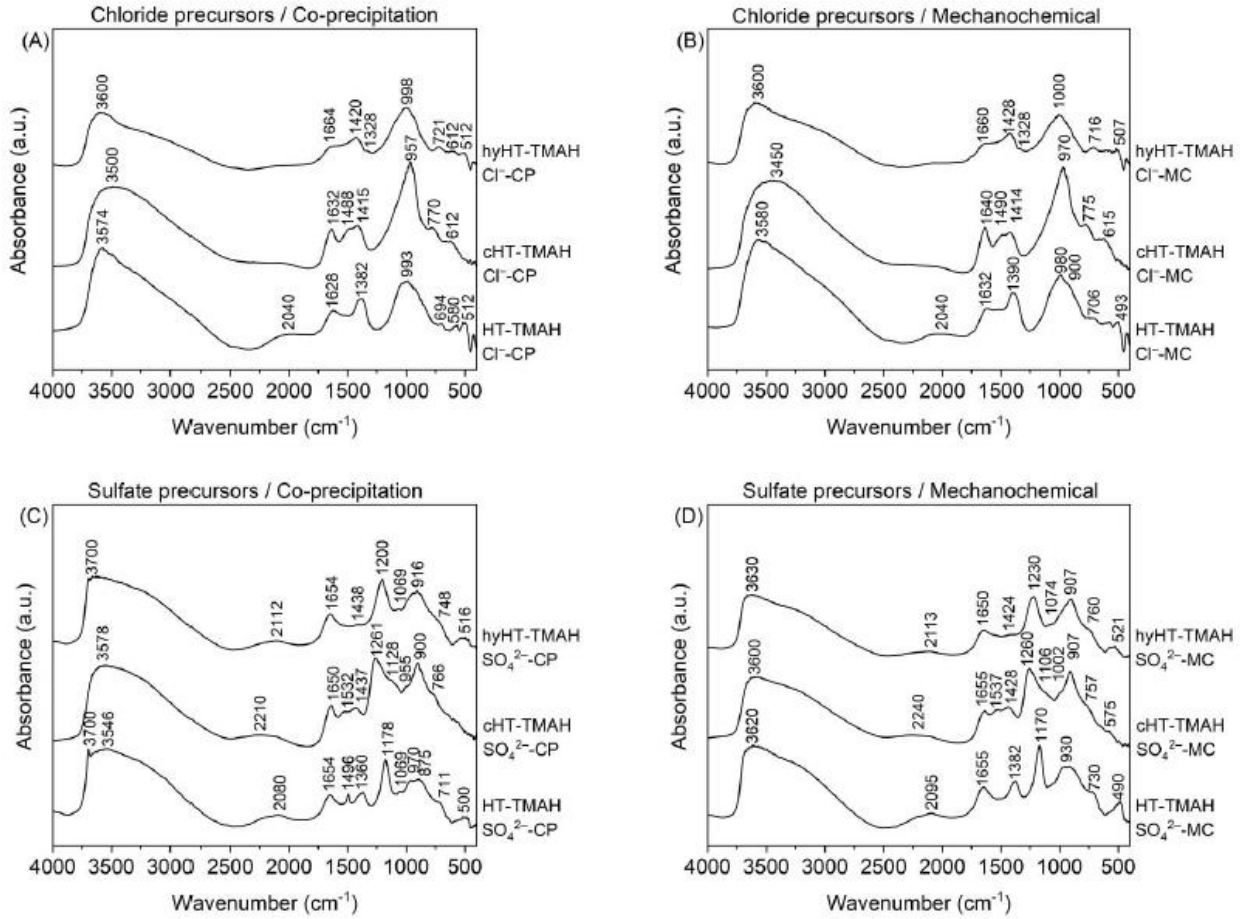

Fig. 2 – The DRIFT of samples prepared by: co-precipitation from chlorides as precursors (A); mechano-chemical from chlorides as precursors (B); co-precipitation from sulfates as precursors (C); and mechano-chemical from sulfates as precursors (D).

However, by calcinations, part of OH^- and CO_3^{2-} groups from hydrotalcites are removed from the structure as CO_2 and H_2O leading to a decrease of the intensity of bands located at 3000 and 1640–1644 cm^{-1}, respectively. However, the presence of these bands confirms that there are remnant carbonate anions, knowing the fact that its complete removal can be obtained at temperatures higher than 650–700 °C, values similar with the disappearance of the memory effect due to migration of the cations from octahedral positions to tetrahedral one.[28] Nevertheless, the hydration of the mixed oxides restored in a greater extent the band at 3000 cm^{-1} and to a lesser extent the band at 1664–1628 cm^{-1} due to insertion of a higher amount of OH^- groups through the memory effect. In the spectra of the hydrotalcite samples prepared from sulfates precursors one can also notice the presence of bands at 1170–1178 cm^{-1} corresponding to (ν_3), at ~1000 cm^{-1} to (ν_1) and ~700 cm^{-1} to (ν_4), under asymmetric and symmetric stretching and bending in SO_4^{2-} anion (Fig. 2C, D black lines).[29] The presence of

sulfate species in the interlayer space, was also confirmed by the larger IFS size of these materials (Table 1). This confirmed the high affinity of this anion for balancing the positive charge in the lamellar layer of hydrotalcite, which already was presented in literature: CO_3^{2-} > SO_4^{2-} > HPO_4^{2-} > OH^- > F^- > Cl^- > Br^- > NO_3^-.[30] The spectra of the corresponding calcined samples show that, similarly to carbonate anions, sulfate is not eliminated during the calcination. However its corresponding bands were shifted to higher wavenumbers due to adopting of a monoclinic configuration.[29] This feature is also noticed in the spectra of the corresponding reconstructed materials. The spectra of the hydrotalcite samples prepared from chloride precursors did not show characteristic bands for metal-chloride bonds.

1.3. UV-Vis characterization

All hydrotalcite samples (black lines) showed a large band around 250 nm that implies the Mg-OH presence in the structure (Fig. 3A–D).[31] Also, the bands at 212 nm for hydrotalcite samples and 215 nm for calcined samples (red lines) indicated the presence of $Mg(OH)_2$ and MgO respectively.[32] For hydrotalcite samples there is also present a common band at 210 nm indicating the presence of the organic base (TMAH) in their structure. This band is much more pronounced for samples prepared from sulfate precursor. The band at 270–290 nm of calcined samples corresponds to Mg-O. As demonstrated in the X-ray patterns, part of this mixed oxides remains as the impurity phase in reconstructed samples. Also, the bands between 237–242 nm correspond to Al-O [33].

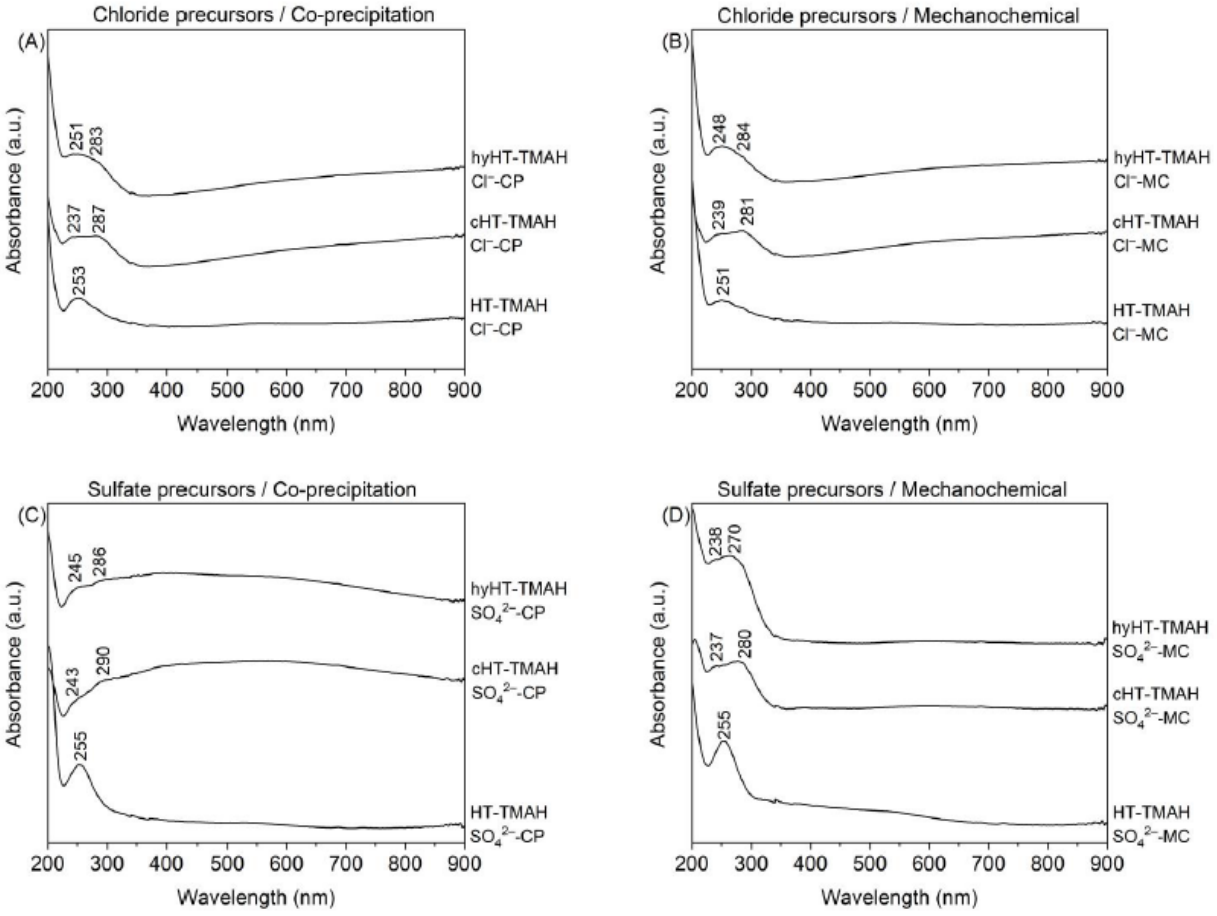

Fig. 3 – DR-UV-Vis spectra of prepared solids by: co-precipitation from chlorides as precursors (A); mechano-chemical from chlorides as precursors (B); co-precipitation from sulfates as precursors (C); and mechano-chemical from sulfates as precursors (D).

1.4. Basicity evaluation

The basicity of samples (Table 2), decreased in the order: mixed oxides > parent hydrotalcite > reconstructed hydrotalcite samples, a trend valid for both strong base sites as well as the sum of weak and medium base sites, regardless of the synthesis route. However, there was a slight increase in basicity for the samples prepared by

mechanochemical route. Also, samples prepared from chloride precursors present a slightly higher basicity value compared to those prepared from sulfate precursors.

Table 2

The basicity of materials

Samples	Total Number of Base Sites (mmol/g) *	Distribution of Base Sites	
		Strong Base Sites (mmol/g) **	Weak and Medium Base Sites (mmol/g) ***
HT-MgAl-Cl^--CP	8.42	0.44	7.98
cHT-MgAl-Cl^--CP	9.88	0.46	9.42
hyHT-MgAl-Cl^--CP	6.93	0.41	6.52
HT-MgAl-Cl^--MC	8.77	0.46	8.31
cHT-MgAl-Cl^--MC	9.89	0.48	9.41
hyHT-MgAl-Cl^--MC	7.01	0.42	6.59
HT-MgAl-SO_4^{2-}-CP	8.25	0.42	7.83
cHT-MgAl-SO_4^{2-}-CP	9.83	0.45	9.38
hyHT-MgAl-SO_4^{2-}-CP	7.92	0.42	7.50
HT-MgAl-SO_4^{2-}-MC	7.23	0.40	6.83
cHT-MgAl-SO_4^{2-}-MC	8.78	0.43	8.35
hyHT-MgAl-SO_4^{2-}-MC	6.71	0.38	6.33

* mmol of acrylic acid
** mmol of phenol
*** the difference between total number of base sites—strong base sites.

1.5. N_2 adsorption-desorption isotherms

The adsorption–desorption isotherms of the parent hydrotalcite samples corresponded to type IV characteristic to mesoporous materials for the samples prepared from chloride precursors (Fig. 4A, B), while III-type isotherms characteristic to macroporous materials were obtained for the samples prepared from sulfate precursors (Fig. 4C, D).

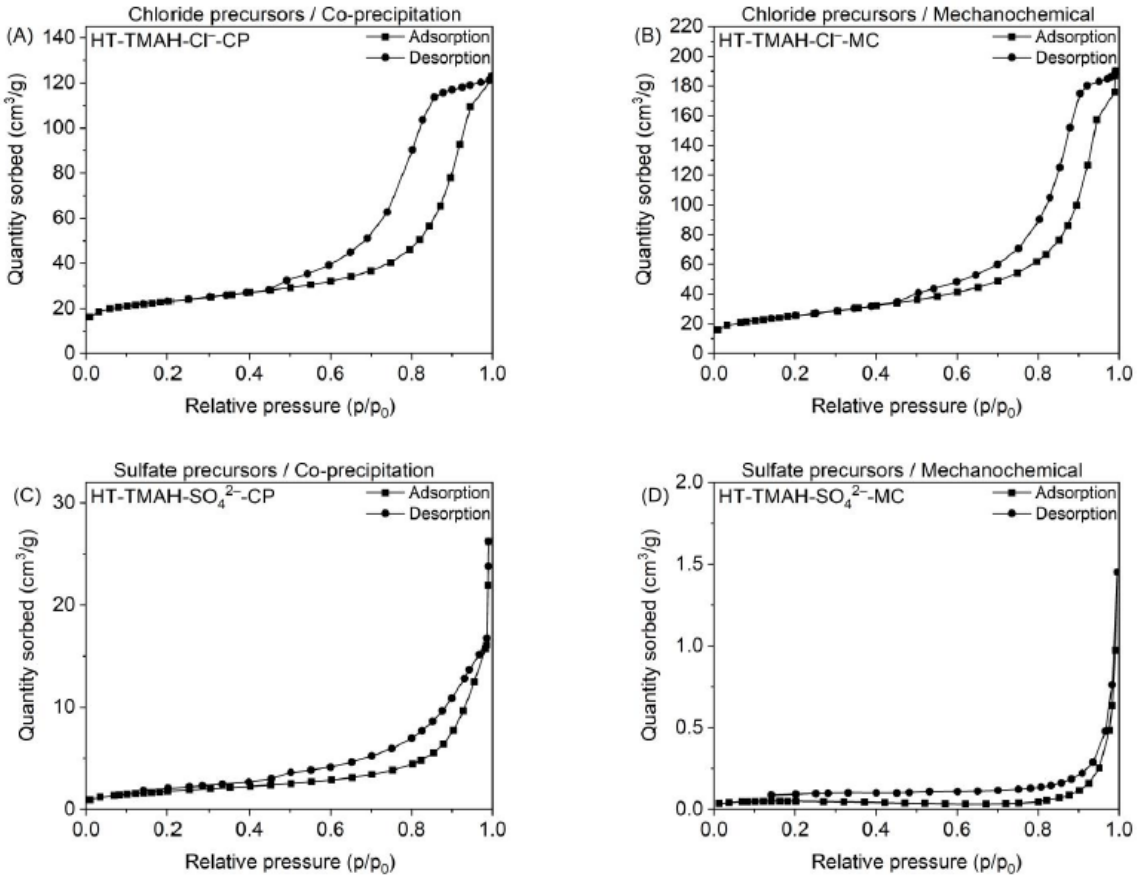

Fig. 4 – Nitrogen adsorption/desorption isotherms at –196 °C for the dried hydrotalcite samples (blue line – adsorption; red line – desorption).

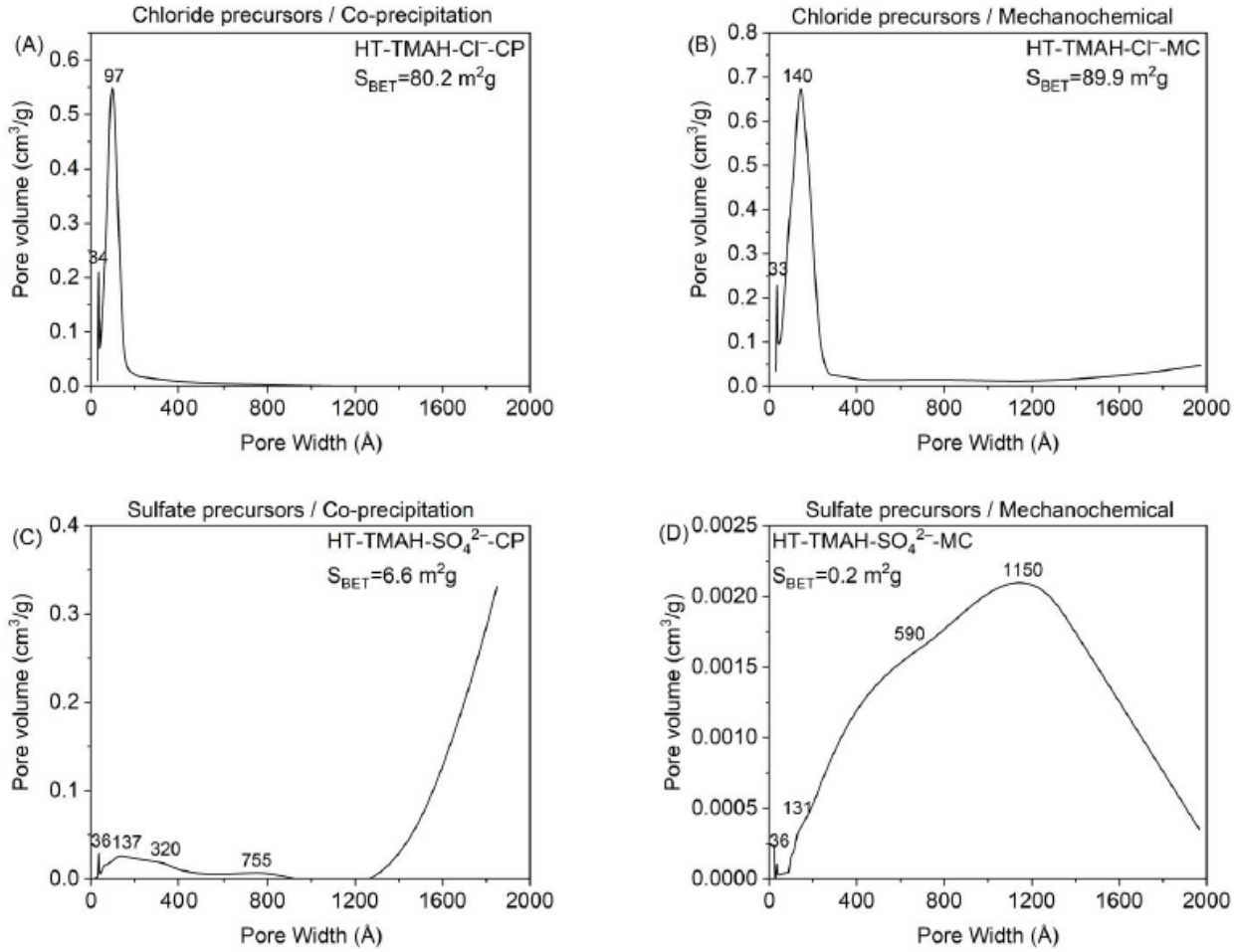

Fig. 5 – The representation of dried sample pore widths (co-precipitation from chlorides as precursors (A); mechano-chemical from chlorides as precursors (B); co-precipitation from sulfates as precursors (C); and mechano-chemical from sulfates as precursors (D)).

2. Catalysts behavior

Blank test shows a poor cyclohexanone conversion of 9.40%, with a selectivity to benzoic acid of 3.13% and an approximately unitary ratio between the *mono*- and *di*-condensation compounds, respectively (Table 3).

The presence of the catalyst leads to a drastic decrease of benzoic acid, also certified by the results of the literature.[17] The trend of the catalytic activity, regardless of the precursor or preparation method used, is: mixed oxides (cHT) > parent hydrotalcite (HT) > reconstructed hydrotalcite (hy-HT) (Table 3). For each set of catalysts (HT, cHT and hyHT) both cyclohexanone conversion and the selectivity to the *di*-condensed product increase with the specific surface area of the catalysts and the total number of base sites, whereas the selectivity to benzoic acid exhibits an opposite behavior. This may be a consequence of the inhibition of the benzaldehyde oxidation in the presence of base sites.[17] Also, the performance in benzaldehyde oxidation to benzoic acid onto LDH materials was already related to the acidity of the catalyst.[34] The best material from catalytic point of view was cHT-TMAH-Cl$^-$-MC, with a conversion of cyclohexanone of 92%, while cHT-TMAH-Cl$^-$-CP showed a conversion of 90%. It was highlighted that the catalytic activity varies linearly with the total number of base sites (Fig. 6). Also, the same trend is observed even for the strong base sites (Fig. 7). If in the case of using chloride precursors, the mechanochemical method brings an increase in the catalytic activity, in the case of sulfate precursors, the opposite behavior is observed, most probably due to its lowest specific surface area. Also, at low basicity values, the selectivity in benzoic acid increases significantly, while the *mono*-/*di*-condensed products ratio is in favor of the *mono*-product in agreement with literature data which showed that the formation of the *mono*-condensed product is favored by acid active sites.[35] At high basicity values, the selectivity is clearly favorable towards the *di*-condensation product.

Table 3

Catalysts behavior in Claisen-Schmidt condensation (benzaldehyde 0.002 moles; cyclohexanone 0.001 moles; solvent-free conditions; 120 °C, the 20 mg catalysts; 2 h)

Samples	Cyclohexanone conversion (%)	Selectivity to benzoic acid (%)	Selectivity to *mono*-condensed product (%)	Selectivity to *di*-condensed product (%)
Blank	9.40	3.13	43.47	53.40
HT-MgAl-Cl^--CP	79.41	8.07	3.36	88.57
cHT-MgAl-Cl^--CP	90.19	3.72	0.52	95.76
hyHT-MgAl-Cl^--CP	47.75	23.09	21.68	55.23
HT-MgAl-Cl^--MC	83.26	3.79	1.20	95.01
cHT-MgAl-Cl^--MC	91.73	3.78	0.16	96.05
hyHT-MgAl-Cl^--MC	48.09	22.89	14.10	63.01
HT-MgAl-SO_4^{2-}-CP	66.84	10.97	8.72	80.31
cHT-MgAl-SO_4^{2-}-CP	87.11	4.61	3.49	91.90
hyHT-MgAl-SO_4^{2-}-CP	64.47	13.63	9.83	76.54
HT-MgAl-SO_4^{2-}-MC	32.70	37.73	32.91	29.36
cHT-MgAl-SO_4^{2-}-MC	66.40	13.92	10.46	75.62
hyHT-MgAl-SO_4^{2-}-MC	28.60	43.89	31.21	24.90

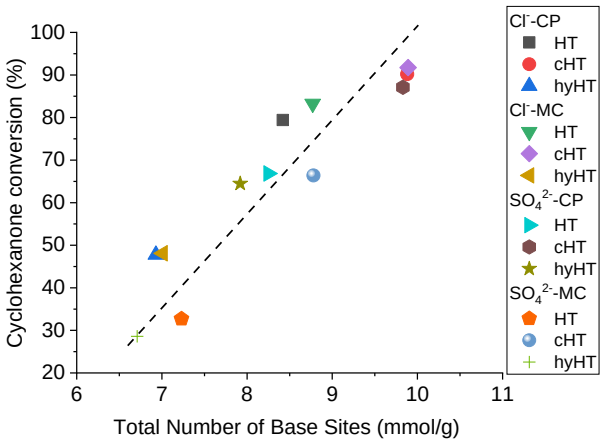

Fig. 6 – The dependence of catalytic activity vs. total base sites.

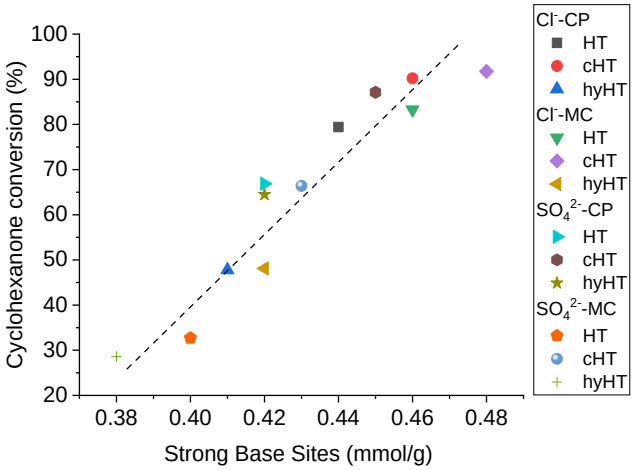

Fig. 7 – The dependence of catalytic activity vs. strong base sites.

The highest yield to the *di*-condensed product (*e.g.* 88%) was obtained with the catalyst cHT-MgAl-Cl^--MC. This value is higher than those obtained with other catalysts under similar reaction conditions such as: MgAl mixed oxide from LDH-nitrate precursors (*e.g.* 85%)[17] and solid base catalyst obtained from fly ash (65%).[26] Other catalysts giving comparable yields to the

di-condensed product were: SmI_3/TMSCl utilized in THF solvent during 8 h at 60 °C (85%),[35] and a hybrid structure based on NaPZeolite/$CoFe_2O_4$ (1:4) combined with aminopyridine (Am-Py) which allowed obtaining 92% yield when the reaction was performed under nitrogen at room temperature.[36]

CONCLUSIONS

Tetra methyl ammonium hydroxide acts both as a synthesis agent and a template agent. The samples obtained from chloride precursors show pores of narrow size, while sulfates generate larger pores. Both the co-precipitation and mechanochemical methods generate the layered structure of hydrotalcites contaminated with traces of $Mg(OH)_2$ and $Al(OH)_3$. Small amounts of TMAH remain in the parent hydrotalcite, being removed by decomposition during the calcination step. By calcination mixed oxides contaminated with MgO are obtained, fact more visible for materials prepared from chlorides precursor. The reconstruction of the parent structure is more evident for materials prepared from chlorides than for those obtained from sulfate as precursors. The variation of the catalytic activity always follows the trend: calcined samples > dried samples > reconstructed samples, similar to the variation of the materials basicity. The decrease in the base character of the samples leads to the increase of the catalytic activity towards the mono-condensation product (2–benzylidene-cyclohexanone) as well as to obtaining a greater amount of benzoic acid. The synthesis of the most active catalyst *e.g.* cHT-MgAl-Cl^--MC is simples and requires lower costs than that of the most active catalyst reported in literature.

Acknowledgements. This work was supported by a grant of the Ministry of Research, Innovation and Digitization, CCCDI-UEFISCDI, project number PN-III-P2-2.1-PED-2021-1870, within PNCDI III. Ana Paula SOARES DIAS acknowledges FCT strategic funding of CERENA (UIDB/ 04028/2020).

REFERENCES

1. S. N. Basahel, S. A. Al‐Thabaiti, K. Narasimharao, N. S. Ahmed and M. Mokhtar, *J. Nanosci. Nanotechnol*, **2014**, *14*, 1931–1946.
2. Y. Huang, C. Liu, S. Rad, H. He and L. Qin, *Processes*, **2022**, *10*, 617.
3. H. Yang, C. Xiong, X. Liu, A. Liu, T. Li, R. Ding, S. P. Shah and W. Li, *Constr. Build. Mater.*, **2021**, *307*, 124991.
4. M. Mohapi, J. S. Sefadi, M. J. Mochane, S. I. Magagula and K. Lebelo, *Crystals*, **2020**, *10*, 957.
5. J. J. Bravo‐Suárez, E. A. Páez‐Mozo and S. T. Oyama, *Quim. Nova*, **2004**, *27*, 601.
6. M. A. Ulibarri, I. Pavlovic, C. Barriga, M. C. Hermosın and J. Cornejo, *Appl. Clay Sci*., **2001**, *18*, 17.
7. K. Takehira, T. Shishido, D. Shouro, K. Murakami, M. Honda, T. Kawabata and K. Takaki, *Appl. Catal. A: Gen*., **2005**, *279*, 41.
8. A. Marchi and C. Apesteguía, *Appl. Clay Sci*., **1998**, *13*, 35.
9. C. A. Barbosa, A. M. D. Ferreira, V. Constantino and A. C. V. Coelho, *J. Incl. Phenom. Macrocycl. Chem.*, **2002**, *42*, 15.
10. F. Teodorescu, A.-M. Pălăduţă and O. D. Pavel, *Mater. Res. Bull*., **2013**, *48*, 2055.
11. F. Cavani, F. Trifiro and A. Vaccari, *Catal. Today*, **1991**, *11*, 173..
12. T. Hibino and H. Ohya, *Appl. Clay Sci*., **2009**, *45*, 123.
13. Z. Liu, R. Ma, M. Osada, N. Iyi, Y. Ebina, K. Takada and T. Sasaki, *J. Am. Chem. Soc*., **2006**, *128*, 4872.
14. L. Jin, X. Zhou, F. Wang, X. Ning, Y. Wen, B. Song, C. Yang, D. Wu, X. Ke and L. Peng, *Nat. Commun*., **2022**, *13*, 6093.
15. L. Liu, Q. Deng, P. White, S. Dong, I. S. Cole, J. Dong and X.-B. Chen, *Corros. Commun*., **2022**, *8*, 40.
16. C. V. Luengo, M. C. Crescitelli, N. A. Lopez and M. J. Avena, *J. Pharm. Sci*., **2021**, *110*, 1779.
17. B. Cojocaru, B. C. Jurca, R. Zăvoianu, R. Bîrjega, V. I. Pârvulescu and O. D. Pavel, *Catal. Commun*., **2022**, *170*, 106485.
18. Y. Zhang, H. Xu and S. Lu, *RSC Adv.*, **2021**, *11*, 24254.
19. D. Jia, D. Jiang, Y. Zheng, H. Tan, X. Cao, F. Liu, L. Yue, Y. Sun and J. Liu, *Nanoscale*, **2019**, *11*, 2812.
20. F. Rong, J. Zhao, Q. Yang and C. Li, *RSC Adv.*, **2016**, *6*, 74536.
21. E. Ciotta, R. Pizzoferrato, M. L. Di Vona, I. V. Ferrari, M. Richetta and A. Varone, *Mater. Sci. Forum*., **2018**, *941*, 2209.
22. R. Karcz, B. D. Napruszewska, A. Walczyk, J. Kryściak-Czerwenka, D. Duraczyńska, W. Płaziński and E. M. Serwicka, *Nanomaterials*, **2022**, *12*, 2775.
23. G. D. Yadav and D. P. Wagh, *Chem. Select*, **2020**, *5*, 9059.
24. E. Rafiee and F. Rahimi, *Monatsh. Chem*., **2013**, *144*, 361.
25. M. Sluban, B. Cojocaru, V. I. Parvulescu, J. Iskra, R. C. Korošec and P. Umek, *J. Catal*., **2017**, *346*, 161.
26. D. Jain, C. Khatri and A. Rani, *Fuel*, **2011**, *90*, 2083.
27. O. D. Pavel, R. Zăvoianu, R. Bîrjega and E. Angelescu, *Catal. Commun*., **2011**, *12*, 845.
28. A. J. Marchi and C. R. Apesteguía, *Appl. Clay Sci*., **1998**, *13*, 35.
29. M. D. Lane, *Am Min*., **2007**, *92*, 1.
30. L. Li, E. Warszawik and P. van Rijn, *Adv. Mater. Interfaces*, **2023**, *10*, 2202396.
31. E. Sheikhhosseini and M. Ranjbar, *OpenNano*, **2019**, *4*, 100028.
32. S. Yousefi, B. Ghasemi, M. Tajally and A. Asghari, *J. Alloys Compd*., **2017**, *711*, 521.
33. P. A. Prashanth, R. S. Raveendra, R. Hari Krishna, S. Ananda, N. P. Bhagya, B. M. Nagabhushana, K. Lingaraju and H. Raja Naika, *J. Asian Ceram. Soc*., **2015**, *3*, 345.
34. X. Wu, X. Xie and Z. Wu, *Prog. React. Kinet. Mech*., **2011**, *36*, 53.
35. Z. Li, Y. Zhang and Q. Li, *J. Chem. Res. S*, **2000**, *12*, 580.
36. Z. Mortezaei, M. Zendehdel and M. A. Bodaghifard, *Res. Chem. Intermed*., **2020**, *46*, 2169.